Chemical Engineering Journal 390 (2020) 124623

Contents lists available at ScienceDirect

Chemical Engineering Journal

journal homepage: www.elsevier.com/locate/cej

Multifunctional polyimide aerogel textile inspired by polar bear hair for thermoregulation in extreme environments

Yujie Wang[a], Ying Cui[a], Ziyu Shao[a], Weiwei Gao[a], Wei Fan[b,*], Tianxi Liu[b], Hao Bai[a,*]

[a] State Key Laboratory of Chemical Engineering, College of Chemical and Biological Engineering, Zhejiang University, Hangzhou 310027, China
[b] State Key Laboratory for Modification of Chemical Fibers and Polymer Materials, College of Materials Science and Engineering, Innovation Center for Textile Science and Technology, Donghua University, 2999 North Renmin Road, Shanghai 201620, China

HIGHLIGHTS

- Overcome fragileness of polyimide aerogels by building biomimetic porous structure.
- The fiber is mechanically strong and highly stretchable at a high porosity.
- The fiber shows excellent thermal insulation property even at up to 500 °C.
- Other functions such as acid alkali resistant and thermoregulation.

ARTICLE INFO

Keywords:
Biomimetic
Freeze-spinning
Polyimide aerogel
Thermal insulating
Fire-retardant
Smart textile

ABSTRACT

Thermoregulating textiles (or protective clothing) are highly demanded for both human health and labor productivity especially in hot working environments. It is challenging to balance wearability and thermal insulating property as they usually demand for opposite porosity. Here, learning from the porous structure of polar bear hair, we report a polyimide aerogel fiber obtained by a freeze-spinning technique. A textile woven with such polyimide fiber is thermally insulating, strong and highly stretchable, fire-retardant (or self-extinguishing), and temperature-resistant. Additionally, it can be readily incorporated with other functions such as acid alkali resistance and thermoregulation by surface modification and infiltration of phase change material. All these properties indicate its potential in protective clothing in hot environments. With the versatility and scalability, our approach paves a new way for fabricating smart textiles with well-defined microstructure and multifunctionality by learning from nature.

1. Introduction

Maintaining body temperature is crucial for human health in daily life [1–3], especially for people who are often exposed to excessive heat stress, such as firefighters and workers in the metallurgy, mining, and glass industry [4,5]. Lack of protection in hot environments usually reduces efficient working time and productivity, and increases the risk in heat-related illness [6]. Therefore, many personal body cooling systems using ice, water, air or phase change materials as the cooling medium were developed [6–10]. However, they are usually limited by the requirement for complex equipment and their heaviness, which largely restrict the mobility of human body. An alternative solution to this critical issue would be a protective clothing that is thermally insulating at elevated temperatures, which can effectively delay the temperature increase in the microclimate near human skin and therefore increase the exposure time.

Porous materials like SiO_2 aerogel [11–14] exhibit excellent thermal insulating performance and heat tolerance, yet suffer from their intrinsic brittleness in wearable applications. Another potential candidate for such protective clothing is heat-resistant polymers such as polyimide [15–18] which can resist up to 500 °C. But making porous fibers and subsequent protective textiles with these polymers is challenging: excellent thermal insulating performance requires high porosity which usually leads to poor mechanical strength, a prerequisite for weaving and wearing.

Polar bears living in the extremely cold Arctic have provided a successful example for balancing wearability and thermal insulating property of porous materials [19–25]. With a well-defined hierarchical architecture featured as aligned shell and randomly porous core [24], the polar bear hair combines both low thermal conductivity

* Corresponding authors.
E-mail addresses: weifan@dhu.edu.cn (W. Fan), hbai@zju.edu.cn (H. Bai).

https://doi.org/10.1016/j.cej.2020.124623
Received 16 October 2019; Received in revised form 16 January 2020; Accepted 29 February 2020
Available online 29 February 2020

(27.8–48.9 $mW{\cdot}m^{-1}{\cdot}K^{-1}$) [22] and high strength (around 300 MPa). Mimicking the architecture found in polar bear hair is non-trivial, as it is challenging to generate aligned porous structure in synthetic fibers using currently available techniques such as melting spinning [26], electrospinning [27] and templating [28].

Here, we report an aerogel textile woven with porous polyimide fibers fabricated by freeze-spinning [24]. The as-prepared textile is thermally insulating, strong and highly stretchable, fire-retardant (or self-extinguishing), and temperature-resistant. In addition, it can be readily incorporated with other functions such as acid alkali resistance and thermoregulation by surface modification and infiltration of phase change material. Our study pushes the frontier of recent research on thermoregulating textiles to high-temperature applications [1–3,29–35]. With the versatility and scalability of the freeze-spinning method, we believe that our study paves a way for fabricating smart textiles with well-defined microstructure and multifunctionality by learning from nature.

2. Experimental section

2.1. Materials

4,4′-Diaminodiphenyl ether (ODA, 98%), N,N-Dimethylacetamide (DMAc, 99.0%), Pyromellitic dianhydride (PMDA, 99%), Triethylamine (TEA, > 99.5%), and 1-Octadecanol (AR) were all provided by Aladdin Chemistry Co., Ltd, China.

2.2. Preparation of poly(amic acid) (PAA) hydrogel

The water-soluble PAA (the precursor of polyimide) was prepared using the previously reported protocol [16]. Specifically, 4.31 g of ODA was first dissolved in 51 g of DMAc. The solution was further mixed with 4.69 g of PMDA by stirring in an ice bath for 5 h. A viscous pale-yellow PAA solution was obtained after adding 2.18 g of TEA dropwise and stirring for another 5 h. The solution was then slowly poured into deionized water to displace the solvent DMAc and washed with deionized water, followed by freeze-drying. The obtained PAA solid (2 g) was successively mixed with 2 g of TEA and 16 g of deionized water. The mixture was stirred for 30 min and kept for gelation at room temperature for at least 2 h to form PAA hydrogel (10% (w/w)). The PAA hydrogel was centrifuged for 15 min at 5 000 rpm to eliminate air bubbles.

2.3. Freeze-spinning and freeze-drying

The PAA fibers were prepared by freeze-spinning and freeze-drying. Briefly, the PAA hydrogel was extruded from a pump-controlled syringe. The hydrogel fiber was then frozen gradually when passing through a copper ring acting as the cold source. By controlling the extruding speed and the temperature of the cold source, the fiber could be frozen at a controllable freezing speed, which determined the inner porous structure of the fiber. Finally, the frozen fibers were collected by a motor with a speed of about 5 m per hour and freeze-dried for 24 h at −60 °C with freeze dryer under 0.05 mbar pressure (Labconco 8811, Kansas City, USA).

2.4. Thermal imidization

The PAA fiber was imidized through heating under nitrogen or argon flow in a tube furnace (OTF-1200X, Hefei KeJing Materials Technology Co., Ltd, China). To ensure complete imidization, the furnace temperature was increased slowly at 2 °C·min^{-1} and maintained at 100, 200, and 300 °C for 30, 30, and 60 min respectively before cooling.

2.5. Characterization on chemical structure of PAA

The chemical structure of PAA was analyzed using a Fourier transform infrared spectroscopy (Nicolet5700, Thermo Electron Corporation, USA).

2.6. Characterization on structural features

The microstructure of the porous polyimide fiber was observed by scanning electron microscopy (SU-3500, Hitachi, Tokyo, Japan) at an acceleration voltage of 5 kV. The pore size was manually measured based on the SEM images. The porosity of fiber was analyzed through mercury-injection test (AutoPore IV 9510, Micromeritics Instruments Corporation, USA).

2.7. Characterization on mechanical properties

Mechanical properties were tested in the tensile mode by an electronic universal testing machine (UTM2102, Shenzhen Suns Technology Stock Co., Ltd, China) with a gauge length of 10 mm at a loading rate of 1.0 mm·min^{-1}. All the fiber samples were cut into 30 mm long segments. The size of textile samples was 5 × 1 cm.

2.8. Characterization on thermal properties

All thermal images were taken by a thermal imager (Fortic 237, Shanghai IRS Inc., China). The working distance was about 20 cm. The thermal conductivity of the polyimide textile was measured with a thermal conductivity meter (TPS 2500S, Shanghai K-Analysis Co., Ltd, China) by piling several pieces of textile. And the size of sample is about 5 × 5 × 0.5 cm^3. For each experimental condition, at least five measurements were performed to obtain statistically reliable values. The samples' temperature was monitored and recorded by a thermocouple connected to a temperature recorder (SIN-R9600, Hangzhou Sinomeasure Automation Technology Co., Ltd, China). The thermogravimetric analysis (TGA) was performed by a simultaneous thermal analyzer (STA, TGA/DSC3+, METTLER TOLEDO, Switzerland). The thermal analysis of polyester thread and 1-Octadecanol was performed by a differential scanning calorimeter (DSC, TA Q200, TA, USA).

2.9. Characterization on fire-retardant properties

The combustion behavior of textiles (10 × 10 cm^2) was characterized by a cone calorimeter (FTT0007, Fire Testing Technology Co., Ltd, UK) according to ISO 5660.

2.10. Fabrication and characterization of superhydrophobic polyimide textile

The polyimide fiber and textile were modified with silica nanoparticle/sol solution to obtain superhydrophobicity. The contact angle was measured using an optical contact angle measurement (OCA 50AF, DataPhysics Instruments GmbH, Germany).

2.11. Fabrication of polyimide textile infiltrated with phase change material

1-Octadecanol was selected as the phase change material. For the infiltration, an as-prepared polyimide textile was immersed into liquid 1-Octadecanol at 70 °C (above its melting temperature) and taken out to cool down at room temperature.

3. Results and discussion

The preparation of biomimetic polyimide aerogel fiber and textile is schematically described in Fig. 1a. Specifically, poly(amic acid) (PAA) fiber with aligned pores was first obtained by freeze-spinning. As

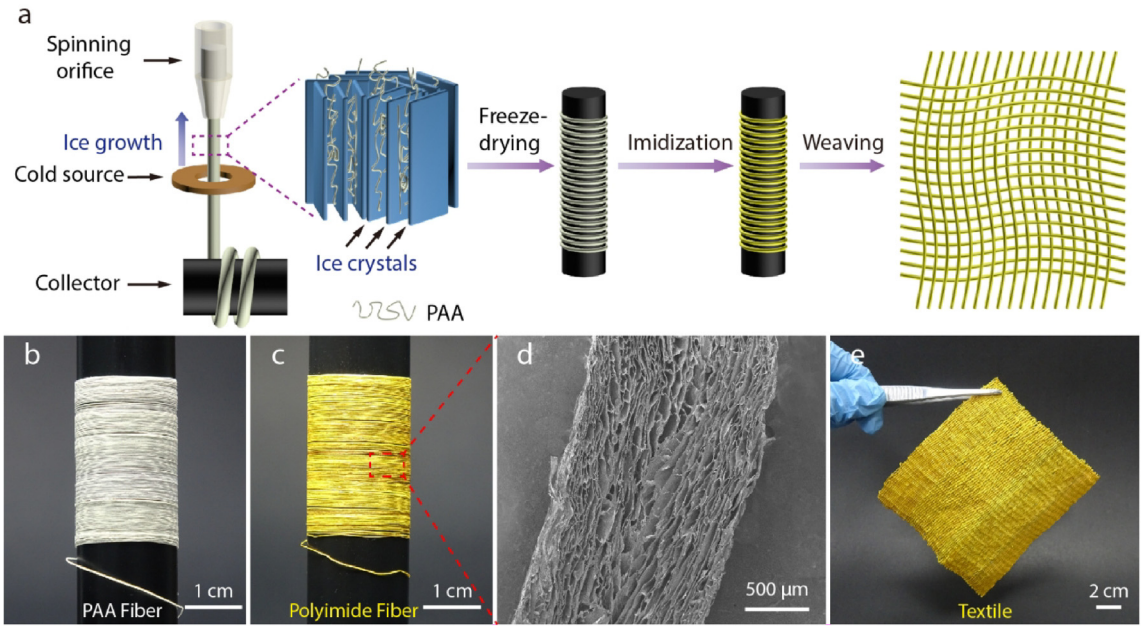

Fig. 1. Continuous and large-scale fabrication of biomimetic polyimide aerogel fiber. (a) Schematic illustration of the preparation of biomimetic polyimide fiber and textile. Porous poly(amic acid) (PAA) fiber was obtained by a freeze-spinning method, followed by thermal imidization to transform into polyimide fiber which was ultimately woven into a textile. (b, c) Optical images of PAA and polyimide fibers respectively. (d) SEM image showing the axial cross-section of the polyimide aerogel fiber in (c). (e) Optical image of a textile (10 × 10 cm^2) woven with the as-prepared polyimide fiber, reflecting its scalability.

polyimide is insoluble in water, we used its water-soluble precursor, poly(amic acid) hydrogel (Fig. S1), to prepare the spinning solution. The PAA fiber reserved its porous structure after the following freeze-drying step. In order to transform PAA into polyimide, a programmed thermal imidization process was implemented. The biomimetic polyimide fiber was then woven into a textile for further test. The as-prepared PAA and polyimide fibers are shown in Fig. 1b and c, respectively. The color change from white to yellow indicates complete imidization of PAA into polyimide. The well-aligned pores obtained during freeze-spinning are reserved in the polyimide fiber as shown in the axial cross-sectional scanning electron microscopy (SEM) image (Fig. 1d). A large piece of textile (10 × 10 cm^2) woven with the as-prepared polyimide fiber can be obtained (Fig. 1e), reflecting the ready scalability of the fabrication process. The density of the polyimide fiber is about 0.2 $g{\cdot}cm^{-3}$, and the porosity is up to 88% according to the mercury-injection test.

As the porous structure of our fiber has a profound impact on its strength and thermal insulating properties, various fibers with distinct pore size were fabricated. Like in a typical ice-templating method, the freezing temperature is critical for the pore size of our polyimide fiber [36–40,46]. As shown by the radial cross-sectional SEM images (Fig. 2a-d), the average pore size of the fiber decreases with decreasing the freezing temperature: from left to right, 70 ± 9.3, 55 ± 10.4, 40 ± 9.7, 25 ± 8.4 μm for freezing at −30, −60, −90, −196 °C (liquid nitrogen), respectively.

With similar porous structure as polar bear hair, our biomimetic polyimide fibers are expected to have excellent thermal insulating property. The as-prepared fibers in Fig. 2a–d were compared by placing them on the same hot stage. A series of infrared images were taken at varying stage temperatures ranging from 25 to 300 °C, with two typical images shown in Fig. 2e for the stage temperature at 25 and 300 °C respectively. The surface temperature of the fibers was then measured based on these infrared images. The corresponding temperature difference ($|\Delta T|$) between the fiber surface and the hot stage was calculated and summarized in Fig. 2f. Fibers with smaller pores show larger $|\Delta T|$ at a given stage temperature, indicating better thermal insulating property. In addition, such distinct capability in insulating heat among fibers become even more remarkable at higher temperatures. For example, when the stage temperature increases from 25 to 300 °C, $|\Delta T|$ for the fiber with the smallest average pore size (25 ± 8.4 μm in Fig. 2d) increases from 2.3 to 78.5 °C.

As polyimide is a temperature-resistant polymer, the as-prepared polyimide fiber was also tested for its fire-retardancy by igniting it with an alcohol lamp (Fig. 2g). Even the fiber surface temperature reaches up to about 700 °C during the burning process (measured from the infrared image), it is self-extinguishing after removal of the alcohol lamp.

As mechanical property is crucial for weaving the biomimetic polyimide fibers into a functional aerogel textile, tensile test was performed. Compared with PAA fiber, the as-prepared polyimide fibers become stronger after thermal imidization but break at a smaller elongation (Fig. S2). For the as-prepared polyimide fibers in Fig. 2a–d, their strength and elongation are highly dependent on their pore size and microstructure (Fig. 2h). The fibers with a medium pore size (40 ± 9.7 μm, prepared at −90 °C) and an aligned porous structure show the highest strength, modulus, and the largest elongation. With a strength up to around 11 MPa, a 300-μm polyimide fiber can even hang up a 100-gram poise (Inset of Fig. 2h).

We further woven the fiber with the best combination of strength and thermal insulating property into a textile. The 500 μm-thick woven textile is both highly stretchable (up to 120% in Fig. 3a and b) and strong (lifting a 400-gram bottled water in Fig. 3c). Quantitatively, the textile shows better tensile strength (14.7 MPa, Fig. 3d) and elongation (86.6%) than a single fiber (10.6 MPa, 28.9%) due to weaving. The mechanical robustness of the textile is crucial for its application as protective clothing.

The thermal insulating property of the polyimide textile was studied comparing with a commercial polyester textile woven in the same way. The polyester thread has similar diameter as the polyimide fiber. These two textiles were placed on the same hot stage to compare their stable surface temperature (Fig. 3e). At varied stage temperatures ranging from 25 to 300 °C, a series of infrared images were taken to measure the average surface temperatures of the textiles. At a stage temperature of 25 °C, the average surface temperature of polyimide and polyester textiles is 23.4 and 23.6 °C respectively, indicating similar thermal insulating property. When the stage temperature is increased to 300 °C,

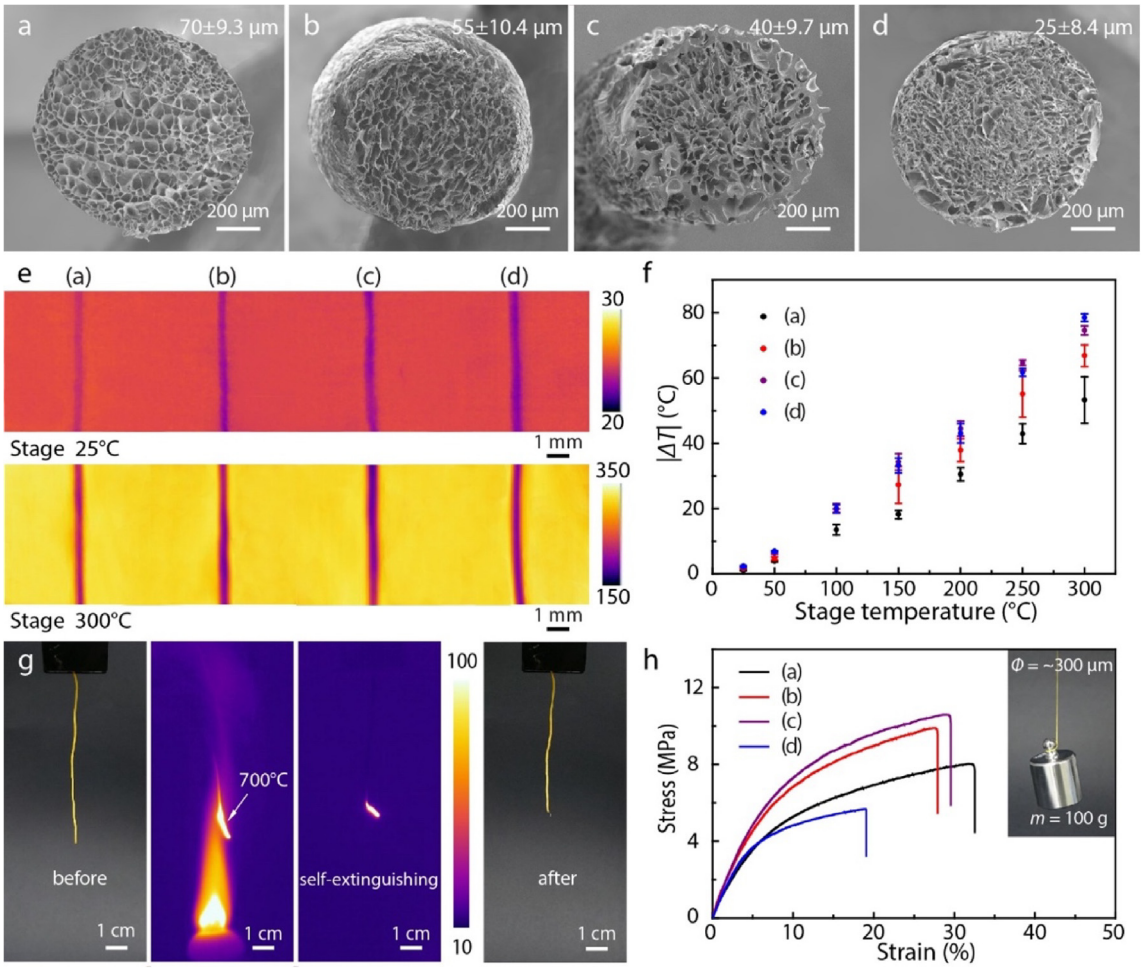

Fig. 2. Microstructure and properties of the biomimetic polyimide aerogel fibers. (a–d) Radial cross-sectional SEM images of various biomimetic polyimide fibers with different porous structure and pore size depending on the freezing temperature. From left to right, the fibers were prepared by freezing at −30, −60, −90, −196 °C, respectively. (e) Infrared images of the as-prepared fibers on a hot stage. Temperatures of the fiber surface were measured based on the infrared images with varying stage temperatures from 25 to 300 °C. (f) Temperature difference ($|\Delta T|$) between the fiber surface and the hot stage plotted against the stage temperature for all the fibers. Those with smaller pores show larger $|\Delta T|$ at a given stage temperature, indicating better thermal insulating property. Such distinct capability in insulating heat becomes even more remarkable at higher temperatures among fibers. (g) Optical and infrared images showing an as-prepared polyimide fiber before and after burning by an alcohol lamp. The temperature scale was set between 10 and 100 °C to ensure the visibility of whole process in infrared images. The fiber reaches a maximum temperature of 700 °C and is self-extinguishing after removing the alcohol lamp. (h) Tensile stress-strain curves of the as-prepared fibers showing different strength and elongation depending on their porous structure. Inset showing a polyimide fiber with 300 μm in diameter hanging a 100 g poise, indicating its high strength.

the polyester textile is already melted while the polyimide textile still exhibits thermal insulating property (with an average surface temperature of 210.5 °C) owing to its temperature resistance. Fig. 3f summarizes the difference between the average surface temperature of both textiles and the hot stage (black dotted line). Larger difference suggests for better thermal insulation. Although both textiles show similar capability in thermal insulation under low temperatures, polyimide textile still shows good thermal insulating property at elevated temperatures while polyester reaches its melting point at around 250 °C (Fig. S3). Quantitatively, the thermal conductivity (λ) of the polyimide textile increases from 36.4 to 160.7 $mW{\cdot}m^{-1}{\cdot}K^{-1}$ when the environmental temperature increases from 25 to 300 °C (Fig. 3g). Similarly, a polyimide foam with similar porous microstructure was also measured for its thermal conductivity, showing an increase from 55.0 to 105.5 $mW{\cdot}m^{-1}{\cdot}K^{-1}$ (Fig. S4). At relatively low temperature, the thermal conductivity of the polyimide textile and foam are close due to their similar porous microstructure. At an elevated temperature of 300 °C, the thermal conductivity of the textile is higher than the foam, which could be attributed to the enhanced heat convection through the pores between the adjacent fibers resulted from weaving. Such a compromise in thermal insulating property for better wearability is acceptable considering that even 160.7 $mW{\cdot}m^{-1}{\cdot}K^{-1}$ is still a low thermal conductivity for most of the temperature-resistant materials [15].

We further demonstrated the potential of using our polyimide textile as thermal protective clothing for workers who often contact hot objects such as molten metal splashes. Fig. 4a shows a plastic finger wearing the polyimide finger-cot (around 4 mm in thickness) touching a hot stage at 300 °C. A polyester finger-cot with similar thickness was also compared. The finger temperature was then recorded by an embedded thermal couple (Fig. 4b). Before touching, the finger temperature is about 19 °C for both cases, reflecting the room temperature. Upon touching, the finger temperature increases rapidly when wearing the polyester finger-cot, reaching around 262 °C within 60 s along with the melting of polyester. In contrast, when wearing the polyimide finger-cot, the finger temperature increases at a much slower speed, reaching an equilibrium at around 132 °C. This delayed temperature increase is beneficial for protective clothing to maintain the microclimate near human skin. After touching for 3 min, the polyester finger-cot is completely destroyed, while the polyimide one barely changes

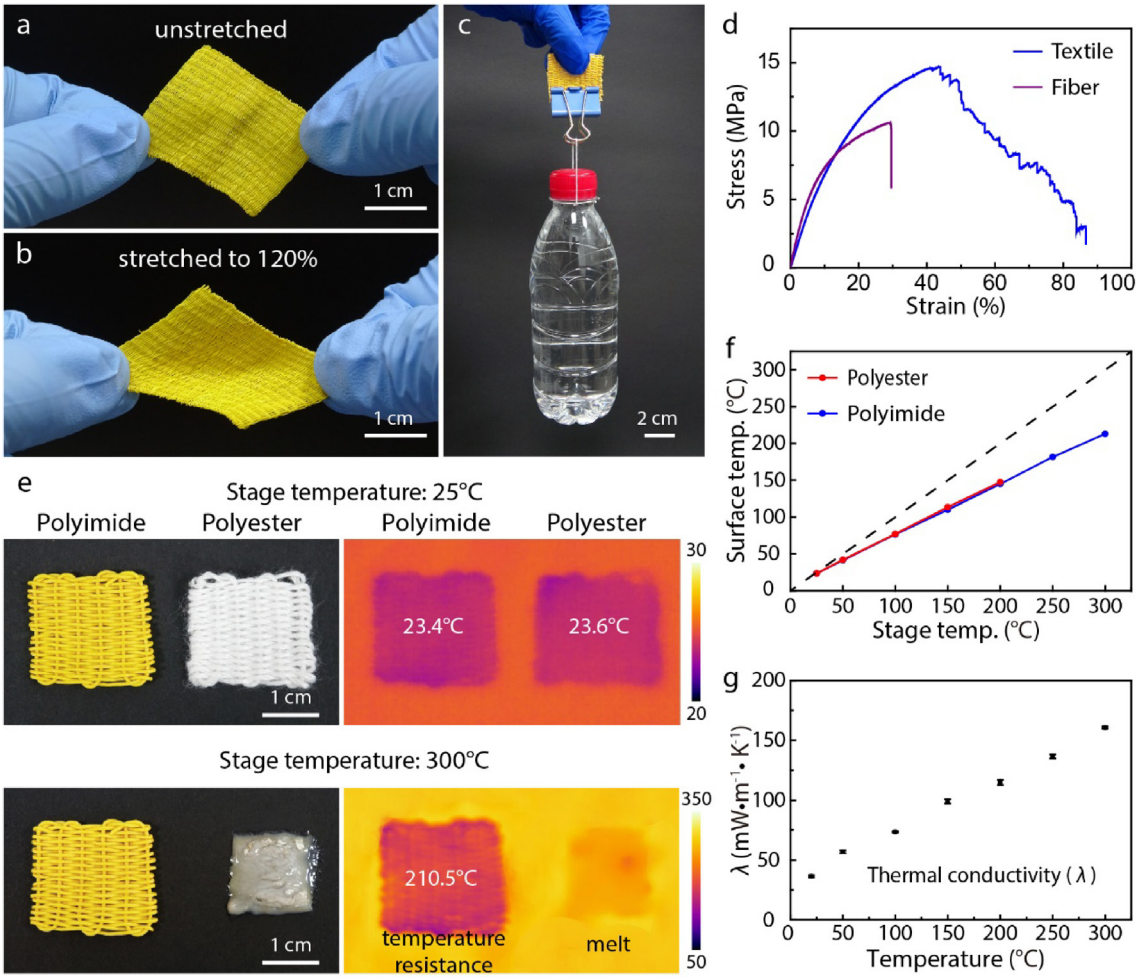

Fig. 3. Mechanical and thermal insulating properties of the textile woven with biomimetic polyimide aerogel fiber. (a–c) Optical images showing the mechanical robustness of the textile. Its high stretchability (up to 120%) and large strength (lifting a 400 g bottled water with a 500 μm-thick textile) are both beneficial for wearing. (d) Tensile stress-strain curves indicating both larger strength and elongation for polyimide textile than fiber. (e) Optical and infrared images of the polyimide and polyester textiles on a hot stage. While the polyester textile is clearly melting at 300 °C, the polyimide textile shows high temperature resistance. (f) The surface temperature of both textiles, measured from the infrared images, were plotted against the stage temperature. Owing to their thermal insulating property, both textiles shows much lower surface temperature than the stage (dotted line). Values for the polyester textile over 250 °C are not adopted as it melts at about 250 °C. (g) Thermal conductivity of the polyimide textile at various environmental temperatures.

(Fig. 4a). The thermal decomposing of both finger-cots was further quantitatively studied by thermogravimetric analysis (TGA) (Fig. S5). The higher decomposing temperature and less weight loss of polyimide textile demonstrate again its better thermal stability compared with polyester.

The self-extinguishing property of polyimide allows our textile to be used as fire-retardant material [41,42]. Both the polyimide and polyester textiles were ignited by an alcohol lamp (Fig. 4c, Movie S1). Upon removal of the flame of the alcohol lamp, the polyimide textile is immediately self-extinguished while the polyester textile is entirely combusted. To quantitatively study the fire-retardancy of both textiles, the cone calorimetry test was performed. As shown in Fig. 4d, the heat release rate of the polyimide textile (with a peak of 92.3 $kW{\cdot}m^{-2}$) is always lower than the polyester (with a peak of 153.2 $kW{\cdot}m^{-2}$). Once ignited, materials with higher heat release rate are always more dangerous, as more heat will be fed back to the material surface leading to accelerated thermal decompose [43]. Consequently, the total heat release (Fig. 4e) of polyester textile (10.1 $MJ{\cdot}m^{-2}$) is much higher than the polyimide textile (3.2 $MJ{\cdot}m^{-2}$). Also, to further indicate the incontestable superiority of the biomimetic polyimide textile for application, characterizations of commercial cotton textile (Fig. S6) are added for comparison. Obviously, the thermal insulating property (Fig. S7) of cotton textile is significantly inferior than that of the biomimetic polyimide textile. Meanwhile, the cotton textile is combustible (Fig. S8), which restricts its application.

In addition to insulate heat at extreme environments up to 500 °C, our polyimide textile is easy to be modified and infiltrated to yield multifunctionality. For example, an acid alkali resistant polyimide textile was obtained by modifying the fiber surface with silica nanoparticle/sol solution (Fig. 5a–e) [44]. The wettability transition of the fiber before and after surface modification is clearly demonstrated by its contact angle (from around 82 to 151°, Fig. 5a and b). Owing to its hydrophobicity, there is no obvious residue on the fiber surface when pulling it from a hanging water droplet (Fig. 5c). The textile woven with these fibers is superhydrophobic (Fig. 5d and S9) and resistant to both alkali and acid solutions (Fig. 5e and f). In contrast, the concentrated sulfuric acid droplet easily penetrates and therefore damages the unmodified polyimide textile (Fig. 5g and h).

In addition to its potential application as the outer layer of a protective clothing facing hot environment, our polyimide textile can be utilized for thermoregulation in the microclimate near human skin when infiltrated with the phase change material (PCM) such as 1-Octadecanol. The aligned porous structure of our polyimide fiber is advantageous for PCM encapsulation [31,45]. Fig. 5i schematically

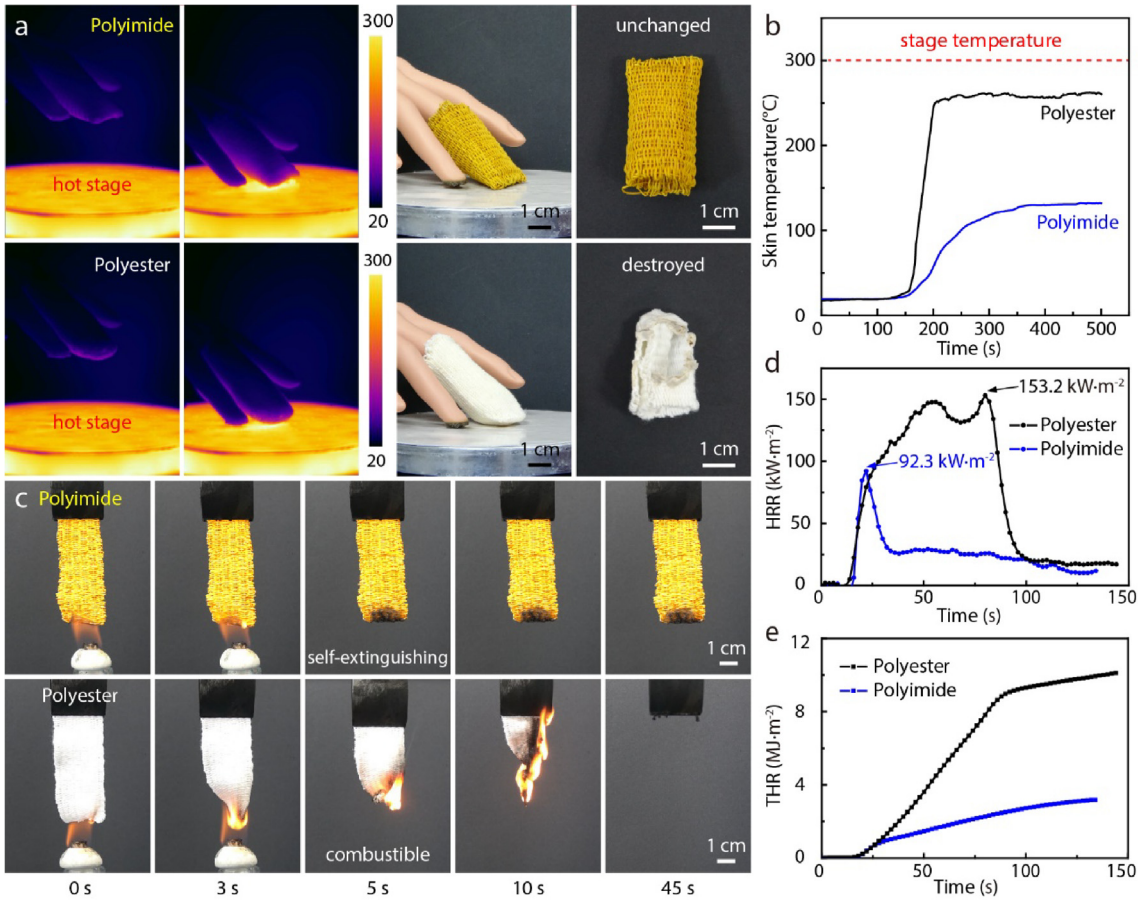

Fig. 4. Thermal insulating and fire-retardant properties of the polyimide aerogel textile. (a) Infrared and optical images showing a plastic finger touching a hot stage at 300 °C, wearing the polyimide and polyester finger-cots (thickness: about 4 mm) respectively. While the polyester finger-cot is severely damaged after touching, the polyimide finger-cot remains unchanged due to the high temperature resistance. (b) Temperature of the finger surface recorded by a thermal couple during the process in (a). A much less temperature increase is recorded when the finger wearing polyimide finger-cot. (c) Optical images for the burning test of polyimide and polyester textiles. While the polyimide textile is fire-retardant, the polyester textile is entirely combusted. (d) Heat release rate curves showing a peak at 92.3 and 153.2 $kW{\cdot}m^{-2}$ for the polyimide and polyester textiles, respectively. (e) Total heat release (THR) curves showing a maximum of 3.2 and 10.1 $MJ{\cdot}m^{-2}$ for the polyimide and polyester textiles, respectively.

illustrates the measurement of the thermoregulating function of the PCM textile placed on a hot stage. The stage was subjected to a heating/cooling cycle between 25 and 100 °C at 25 $°C{\cdot}min^{-1}$. The average temperature of the textile and stage was measured from the infrared images in Fig. 5j and plotted in Fig. 5k. Compared with the linear temperature change of the hot stage and pure polyimide textile (Fig. S10), two plateaus at around 55 °C can be attributed to the phase change of 1-Octadecanol (Fig. S11). The obvious delay and narrower temperature fluctuation clearly demonstrate the thermoregulating function of the PCM textile. During this change it can absorb, store or release large amounts of energy in the form of latent heat.

4. Conclusions

In summary, we demonstrate that polyimide aerogel fiber mimicking polar bear hair can be fabricated by a facile freeze-spinning method. Owing to its special microstructure and the intrinsic high temperature resistance of polyimide, the textile woven with such fiber possesses excellent thermal insulating property, especially at high temperature. Moreover, it is easy to be modified and infiltrated to yield multifunctionality such as acid alkali resistance and thermoregulating capability. Together with its wearability and self-extinguishing property, our polyimide textile holds great potential as thermoregulating textile at high temperature. With the versatility and scalability of our approach, we believe that our study points to a future direction in designing smart textiles with well-defined microstructure and various functionalities by learning from nature.

Author contributions

H. Bai conceived the concept and supervised the project. H. Bai, W. Fan, T. Liu and W. Gao designed the experiments. H. Bai, Y. Wang, and W. Fan wrote the manuscript. Y. Wang, Y. Cui, and Z. Shao performed the experiments. Experimental results were collected and analyzed through contributions of all authors.

Declaration of Competing Interest

The authors declare no competing financial interest.

Acknowledgments

This work was supported by the National Natural Science Foundation of China (No. 51722306, 51603182, 21674098, and 21674019), the National Key Research and Development Program of China (2017YFC1103900), the Fundamental Research Funds for the Central Universities (No. 2018XZZX002-15), Shanghai Sailing Program (17YF1400200), and Ministry of Education of the People's Republic of China (6141A0202202).

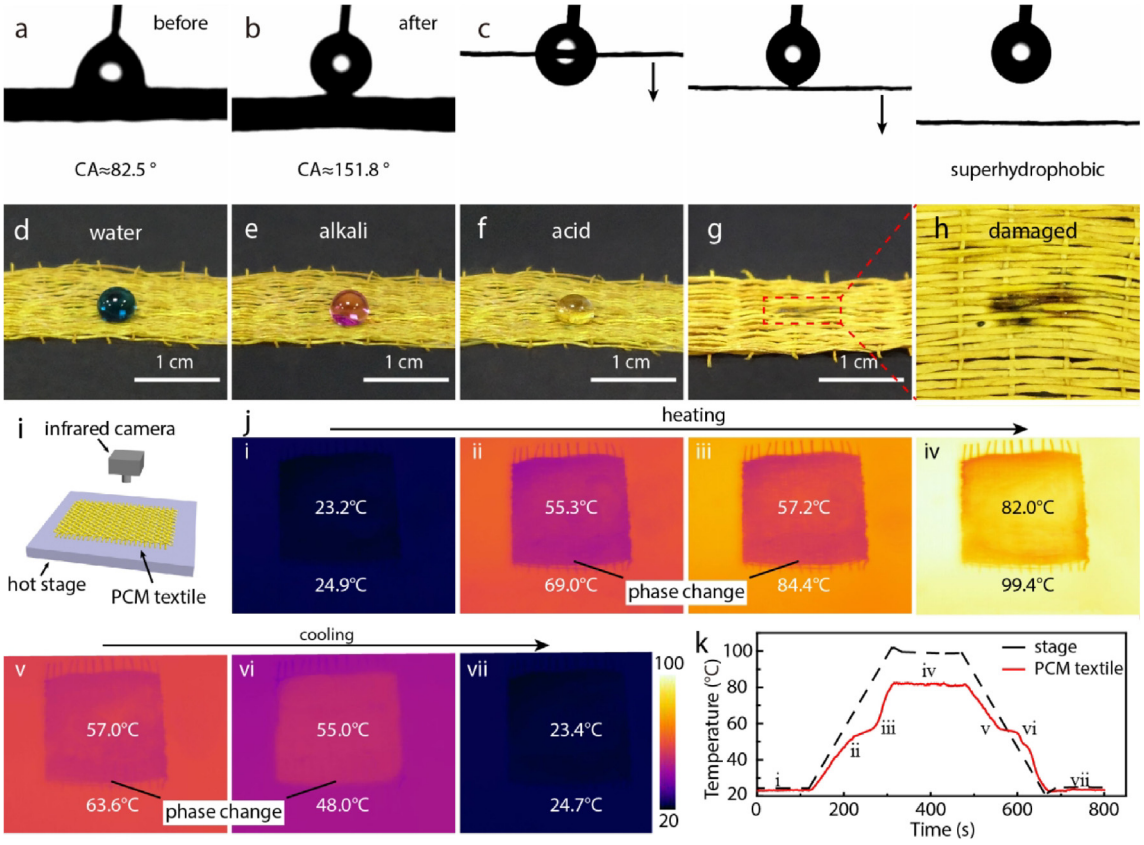

Fig. 5. Multifunctionality of the biomimetic polyimide fiber and textile. (a, b) Optical images showing the contact angles of the polyimide fiber before and after surface modification. (c) Optical images recorded when pulling out a superhydrophobic polyimide fiber from a water droplet indicating low hysteresis of water on the fiber surface. Optical images showing the (d) superhydrophobicity and (e, f) acid alkali resistance of the modified polyimide textile. The liquid droplets were dyed for better visualization. (g, h) Concentrated sulfuric acid easily spreads and damages the unmodified polyimide textile. (i) Schematic illustration and (j) infrared images showing the thermoregulating function of the polyimide textile infiltrated with phase change material during a heating and cooling cycle (between 25 and 100 ˚C). The temperatures in each image corresponds to the average surface temperature of the textile and the hot stage respectively. (k) Comparison between the temperature variation of the textile (red solid line) and stage (black dotted line) showing obvious delay and narrower temperature fluctuation for the polyimide textile infiltrated with phase change material during the heating and cooling cycle. (For interpretation of the references to color in this figure legend, the reader is referred to the web version of this article.)

Appendix A. Supplementary data

Supplementary data to this article can be found online at https://doi.org/10.1016/j.cej.2020.124623.

References

[1] X.A. Zhang, S. Yu, B. Xu, M. Li, Z. Peng, Y. Wang, S. Deng, X. Wu, Z. Wu, M. Ouyang, Y.H. Wang, Dynamic gating of infrared radiation in a textile, Science 363 (2019) 619–623.

[2] P.C. Hsu, A.Y. Song, P.B. Catrysse, C. Liu, Y. Peng, J. Xie, S. Fan, Y. Cui, Radiative human body cooling by nanoporous polyethylene textile, Science 353 (2016) 1019–1023.

[3] P.C. Hsu, C. Liu, A.Y. Song, Z. Zhang, Y. Peng, J. Xie, K. Liu, C.L. Wu, P.B. Catrysse, L. Cai, S. Zhai, A. Majumdar, S. Fan, Y. Cui, A dual-mode textile for human body radiative heating and cooling, Sci. Adv. 3 (2017) e1700895.

[4] T. Kjellstrom, I. Holmer, B. Lemke, Workplace heat stress, health and productivity – an increasing challenge for low and middle-income countries during climate change, Glob. Health. Action 2 (2009) 46–51.

[5] W.L. Kenney, D.W. DeGroot, L.A. Holowatz, Extremes of human heat tolerance: life at the precipice of thermoregulatory failure, J. Therm. Biol. 29 (2004) 479–485.

[6] M.M. Yazdi, M. Sheikhzadeh, Personal cooling garments: a review, J. Text. I 105 (2014) 1231–1250.

[7] J. Smolander, K. Kuklane, D. Gavhed, H. Nilsson, I. Holmer, Effectiveness of a light-weight ice-vest for body cooling while wearing fire fighter's protective clothing in the heat, Int. J. Occup. Saf. Ergon. 10 (2004) 111–117.

[8] G. Bartkowiak, A. Dabrowska, A. Marszalek, Assessment of an active liquid cooling garment intended for use in a hot environment, Appl. Ergon. 58 (2017) 182–189.

[9] T.D. Chinevere, B.S. Cadarette, D.A. Goodman, B.R. Ely, S.N. Cheuvront, M.N. Sawka, Efficacy of body ventilation system for reducing strain in warm and hot climates, Eur. J. Appl. Physiol. 103 (2008) 307–314.

[10] G. Bartkowiak, A. Dabrowska, A. Marszałek, Analysis of thermoregulation properties of PCM garments on the basis of ergonomic tests, Text. Res. J. 83 (2013) 148–159.

[11] S. Xu, L. Chen, M. Gong, X. Hu, X. Zhang, Z. Zhou, Characterization and engineering application of a novel ceramic composite insulation material, Compos. Part B: Eng. 111 (2017) 143–147.

[12] Z.-L. Yu, N. Yang, V.A. Kalkavoura, B. Qin, Z.-Y. Ma, W.-Y. Xing, C. Qian, L. Bergstrom, M. Antonierri, S.-H. Yu, Fire-retardant and thermally insulating phenolic-silica aerogels, Angew. Chem. Int. Ed. 130 (2018) 4628–4632.

[13] F. Hu, S. Wu, Y. Sun, Hollow-structured materials for thermal insulation, Adv. Mater. (2018) e1801001.

[14] L. Su, H. Wang, M. Niu, X. Fan, M. Ma, Z. Shi, S.W. Guo, Ultralight, recoverable, and high-temperature-resistant SiC nanowire aerogel, ACS Nano 12 (2018) 3103–3111.

[15] I. Gouzman, E. Grossman, R. Verker, N. Atar, A. Bolker, N. Eliaz, Advances in polyimide-based materials for space applications, Adv. Mater. 31 (2019) e1807738.

[16] W. Fan, L. Zuo, Y. Zhang, Y. Chen, T. Liu, Mechanically strong polyimide / carbon nanotube composite aerogels with controllable porous structure, Compos. Sci. Technol. 156 (2018) 186–191.

[17] X. He, L. Zhang, D. Meng, J. Wu, From hydrogel to aerogel: A green fabrication of multifunctional polyimide absorbents, Eur. Polym. J. 89 (2017) 461–467.

[18] L. Zhang, J. Wu, X. Zhang, G. Gong, J. Liu, L. Guo, Multifunctional, marvelous polyimide aerogels as highly efficient and recyclable sorbents, RSC Adv. 5 (2015) 12592–12596.

[19] T. Stegmaier, M. Linke, H. Planck, Bionics in textiles: flexible and translucent thermal insulations for solar thermal applications, Philos. Trans. R. Soc. A 367 (2009) 1749–1758.

[20] N. Zhao, Z. Wang, C. Cai, H. Shen, F. Liang, D. Wang, C. Wang, T. Zhu, J. Guo, Y. Wang, X. Liu, C. Duan, H. Wang, Y. Mao, X. Jia, H. Dong, X. Zhang, J. Xu, Bioinspired materials: from low to high dimensional structure, Adv. Mater. 26 (2014) 6994–7017.

[21] P. Tao, W. Shang, C. Song, Q. Shen, F. Zhang, Z. Luo, N. Yi, D. Zhang, T. Deng, Bioinspired engineering of thermal materials, Adv. Mater. 27 (2015) 428–463.

[22] A. Du, H. Wang, B. Zhou, C. Zhang, X. Wu, Y. Ge, T. Niu, X. Ji, T. Zhang, Z. Zhang,

G. Wu, J. Shen, Multifunctional silica nanotube aerogels inspired by polar bear hair for light management and thermal insulation, Chem. Mater. 30 (2018) 6849–6857.
[23] A. August, A. Kneer, A. Reiter, M. Wirtz, J. Sarsour, T. Stegmaier, S. Barbe, G.T. Gresser, B. Nestler, A bionic approach for heat generation and latent heat storage inspired by the polar bear, Energy 168 (2019) 1017–1030.
[24] Y. Cui, H. Gong, Y. Wang, D. Li, H. Bai, A thermally insulating textile inspired by polar bear hair, Adv. Mater. 30 (2018) e1706807.
[25] H.-J. Zhan, K.-J. Wu, Y.-L. Hu, J.-W. Liu, H. Li, X. Guo, J. Xu, Y. Yang, Z.-L. Yu, H.-L. Gao, X.-S. Luo, J.-F. Chen, Y. Ni, S.-H. Yu, Biomimetic carbon tube aerogel enables super-elasticity and thermal insulation, Chem 5 (2019) 1–12.
[26] S.P. Rwei, Formation of hollow fibers in the melt-spinning process, J. Appl. Polym. Sci. 82 (2001) 2896–2902.
[27] N. Bhardwaj, S.C. Kundu, Electrospinning: a fascinating fiber fabrication technique, Biotechnol. Adv. 28 (2010) 325–347.
[28] S. Cao, Y. Zhang, D. Zhang, J. Fan, J. Zhang, J. Zhou, J. Zhang, Micrometer-scale kirkendall effect in the formation of high-temperature-resistant Cr2O3/Al2O3 solid solution hollow fibers, Chem. Mater. 30 (2018) 5978–5986.
[29] T. Jia, Y. Wang, Y. Dou, Y. Li, M.J. Andrade, R. Wang, S. Fang, J. Li, Z. Yu, R. Qian, Z. Liu, Y. Cheng, Y. Su, M.M. Jolandan, R.H. Baughman, D. Qian, Z. Liu, Moisture sensitive smart yarns and textiles from self-balanced silk fiber muscles, Adv. Funct. Mater. (2019) 1808241.
[30] J.K. Tong, X. Huang, S.V. Boriskina, J. Loomis, Y. Xu, G. Chen, Infrared-transparent visible-opaque fabrics for wearable personal thermal management, ACS Photonics 2 (2015) 769–778.
[31] G. Li, G. Hong, D. Dong, W. Song, X. Zhang, Multiresponsive graphene-aerogel-directed phase-change smart fibers, Adv. Mater. 30 (2018) 1801754.
[32] J. Lyu, Z. Liu, X. Wu, G. Li, D. Fang, X. Zhang, Nanofibrous kevlar aerogel films and their phase-change composites for highly efficient infrared stealth, ACS Nano 13 (2019) 2236–2245.
[33] P. Liu, Y. Li, Y. Xu, L. Bao, L. Wang, J. Pan, Z. Zhang, X. Sun, H. Peng, Stretchable and energy-efficient heating carbon nanotube fiber by designing a hierarchically helical structure, Small 14 (2018) 1702926.
[34] T. Gao, Z. Yang, C. Chen, Y. Li, K. Fu, J. Dai, E.M. Hitz, H. Xie, B. Liu, J. Song, B. Yang, L. Hu, Three-dimensional printed thermal regulation textiles, ACS Nano 11 (2017) 11513–11520.
[35] Y. Guo, C. Dun, J. Xu, J. Mu, P. Li, L. Gu, C. Hou, C.A. Hewitt, Q. Zhang, Y. Li, D.L. Carroll, H. Wang, Ultrathin, washable, and large-area graphene papers for personal thermal management, Small 13 (2017) 1702645.
[36] G. Du, A. Mao, J. Yu, J. Hou, N. Zhao, J. Han, Q. Zhao, W. Gao, T. Xie, H. Bai, Nacre-mimetic composite with intrinsic self-healing and shape-programming capability, Nat. Commun. 10 (2019) 800.
[37] J. Han, G. Du, W. Gao, H. Bai, An anisotropically high thermal conductive boron nitride/epoxy composite based on nacre-mimetic 3D network, Adv. Funct. Mater. 29 (2019) 1900412.
[38] M. Yang, N. Zhao, Y. Cui, W. Gao, Q. Zhao, C. Gao, H. Bai, T. Xie, Biomimetic architectured graphene aerogel with exceptional strength and resilience, ACS Nano 11 (2017) 6817–6824.
[39] W. Gao, N. Zhao, W. Yao, Z. Xu, H. Bai, C. Gao, Effect of flake size on the mechanical properties of graphene aerogels prepared by freeze casting, RSC Adv. 7 (2017) 33600–33605.
[40] N. Zhao, M. Yang, Q. Zhao, W. Gao, T. Xie, H. Bai, Superstretchable nacre-mimetic graphene/poly(vinyl alcohol) composite film based on interfacial architectural engineering, ACS Nano 11 (2017) 4777–4784.
[41] X.H. Shi, Y.J. Xu, J.W. Long, Q. Zhao, X.M. Ding, L. Chen, Y.Z. Wang, Layer-by-layer assembled flame-retardant architecture toward high-performance carbon fiber composite, Chem. Eng. J. 353 (2018) 550–558.
[42] B. Wicklein, A. Kocjan, G.S. Alvarez, F. Carosio, G. Camino, M. Antonietti, L. Bergstrom, Thermally insulating and fire-retardant lightweight anisotropic foams based on nanocellulose and graphene oxide, Nat. Nanotechnol. 10 (2015) 277–283.
[43] W.C. Wei, C. Deng, S.C. Huang, Y.X. Wei, Y.Z. Wang, Nickel-Schiff base decorated graphene for simultaneously enhancing the electroconductivity, fire resistance, and mechanical properties of a polyurethane elastomer, J. Mater. Chem. 6 (2018) 8643–8654.
[44] D. Ge, L. Yang, Y. Zhang, Y. Rahmawan, S. Yang, Transparent and super-amphiphobic surfaces from one-step spray coating of stringed silica nanoparticle/sol solutions, Part. Part. Syst. Char. 31 (2014) 763–770.
[45] N. Sarier, E. Onder, Organic phase change materials and their textile applications: an overview, Thermochim. Acta 540 (2012) 7–60.
[46] Y. Cui, Y. Wang, Z. Shao, A. Mao, W. Gao, H. Bai, Smart sponge for fast liquid absorption and thermal responsive self-squeezing, Adv. Mater. (2020) e1908249In press.